
Article:
Tu, R., Gitman, I. and Susmel, L. (2022) Fuzzy inference system for failure strength estimation of plain and notched 3D-printed polylactide components. Fatigue and Fracture of Engineering Materials & Structures, 45 (6). pp. 1663-1677. ISSN: 8756-758X

https://doi.org/10.1111/ffe.13689

Received: 22 December 2021 | Revised: 3 March 2022 | Accepted: 8 March 2022

DOI: 10.1111/ffe.13689

ORIGINAL ARTICLE

FFEMS Fatigue & Fracture of Engineering Materials & Structures WILEY

Fuzzy inference system for failure strength estimation of plain and notched 3D-printed polylactide components

Ruixuan Tu[1] | **Inna Gitman**[2] | **Luca Susmel**[3]

[1]Department of Mechanical Engineering, University of Sheffield, Sheffield, UK

[2]Department of Mechanics of Solids, Surfaces & Systems, University of Twente, Enschede, The Netherlands

[3]Department of Civil and Structural Engineering, University of Sheffield, Sheffield, UK

Correspondence
Ruixuan Tu, Engineering Heartspace, Sir Frederick Mappin Building, Mappin Street, University of Sheffield, Sheffield S1 3JD, UK.
Email: rtu1@sheffield.ac.uk

Funding information
EC Horizon 2020 MSCA-RISE-2016 FRAMED Fracture across Scales and Materials, Processes and Disciplines

Abstract

A fuzzy sets based computational fuzzy inference system has been used to estimate the failure strength of 3D-printed polylactide components. The research has confirmed and validated the accuracy and reliability of this approach with a satisfying level of reliability. As far as failure strength is concerned, the following two types of input parameters have been considered: (i) manufacturing variables (i.e., manufacturing angle, infill density, and size of manufacturing voids) and (ii) geometrical features (i.e., notch root radius). The individual significance of the various parameters under investigation has been identified together with the influence on the estimation accuracy of the number of specimens being used. The fuzzy inference system has shown an accuracy improvement compared to the failure strength estimation, obtained as a result of an existing analytical method. The fuzzy inference system approach has also been shown to have a good potential as a decision-making tool in design problems.

KEYWORDS

3D printing, estimation accuracy, failure strength, fuzzy inference system, fuzzy sets

1 | INTRODUCTION

Additive manufacturing is one of those novel technologies which allow objects to be manufactured by depositing and solidifying materials layer by layer. Compared with conventional subtractive technique, 3D printing leads to less material waste and usage. Depending on manufacturing technologies, different materials can be used in 3D printing, such as ceramics,[1] metals,[2] or thermoplastics.[3] One of the most common 3D printing materials is polylactide (PLA), which is biodegradable and can be manufactured at a low cost from renewable resources such as corn starch and sugarcane, making it economically and environmentally sustainable. PLA has a relatively low melting temperature (around 180°C),[4] which clearly makes it suitable for 3D printing.

One of the basic technologies used to 3D-print polymers is the so-called fused deposition modeling (FDM). The FDM requires the use of a heated nozzle through which material filaments are melted and extruded onto the build plate.[5] As the filament cools down and hardens, it is deposited along with the horizontal movement of the nozzle, creating a desired geometry in the layer. The internal geometry of printed layers can be in form of various infill patterns (triangle, square, honeycomb, hexagon, etc.). With one layer finished, the build plate goes down so that the filament can be deposited on top of the existing layer, forming the 3D structure.

During the 3D printing process, there are multiple manufacturing parameters that can be changed and controlled individually. In the following sections, attention will be focused mainly on two particular manufacturing parameters, namely, infill density and manufacturing angle (introduced in Section 2) which can strongly affect the strength performance of 3D-printed objects.

Apart from the two parameters introduced above, there are other manufacturing specifications that affect the strength performance of 3D-printed objects such as printing direction,[6] layer thickness,[7] nozzle temperature,[8] and feed rate.[7]

One of the key aspects associated with additive manufacturing is that 3D-printed materials can be characterized by an evident level of anisotropy.[9] This manufacturing-related anisotropy is seen to affect their overall mechanical response,[9] with this holding true under both static[10] and fatigue loading.[11–13] In this context, as far as the mechanical behavior of 3D-printed polymers (such as, for instance, ABS and PLA) is concerned, much experimental evidence suggests that, certainly, the anisotropy associated with the building direction plays a role of primary importance.[14–17] For instance, it is seen from the experiments that the ultimate tensile strength and the yield stress of 3D-printed ABS/PLA manufactured perpendicularly to the build plate are lower than the corresponding mechanical properties that are obtained when objects are manufactured either on-edge or flat.[14,15] Similarly, when components are fused-filament fabricated flat on the built plate, their mechanical response is influenced by the intrinsic anisotropy resulting from the value being set for the manufacturing raster angle.[16,17] In more detail, the mechanical performance of 3D-printed polymers is seen to be higher when the loading is applied along directions that are parallel to the 3D-printed filaments. This is because under the above circumstances the overall mechanical response of additively manufactured polymers mainly depends on the axial mechanical strength of the extruded filaments.[14–17] In contrast, when the loading is applied along directions that are perpendicular to the 3D-printed filaments, the overall strength of the polymer under investigation markedly depends on the forces bonding together adjacent filaments/layers. Since, by their nature, these bonding forces result in a lower mechanical performance/strength than the corresponding mechanical performance/strength characterizing the extruded filaments themselves, overall 3D-printed materials are seen to be weaker when the loading is applied along a direction perpendicular to the direction of the filaments.[15]

Multiple possible combinations of the manufacturing parameters briefly discussed above make it very difficult for the strength to be estimated in conventional ways which are based on building empirical relations and material models.[18] These models and relationships rely on previous knowledge and a large quantity of costly and time-consuming experiments. At the same time, they become less flexible and more complex due to a large number of aforementioned possible combinations of manufacturing parameters. Therefore, in recent years, the international scientific community has made a big effort to formulate alternative approaches such as data-driven methods. Data-driven methods learn from a group of existing raw data and can estimate the behavior of required variables based on this previous learning process. One of these data-driven approaches is known as fuzzy inference system (FIS) which is based on the theory of fuzzy sets. In what follows, this FIS framework will be used to perform the failure strength assessment of 3D-printed plain and notched components of PLA.

In Section 2, details on the manufacturing of the 3D-printed specimens (plain and notched) being considered will be presented for the readers' benefit. Section 3 will introduce and discuss the theory of FIS methodology in detail, going through all necessary steps to build up FIS models. Section 4 will adapt the generic FIS model to the 3D-printed plain specimens being considered in the present investigation. Subsequently, the FIS approach being devised will be tested and validated, with this being done to discuss the influence of the number of tests as well as of the key manufacturing parameters on the estimation accuracy. Section 5 will analyze 3D-printed notched specimens, looking at both manufacturing and geometrical parameters and comparing the performance of FIS with reported previously analytical methodologies.

2 | MANUFACTURING OF 3D-PRINTED COMPONENTS

Not being itself the main focus of this paper, the manufacturing process of 3D-printed specimens deserves a special attention. In this section, some important terminology and necessary variables used in what follows will be introduced.

As mentioned in Section 1, two different geometries will be used in our investigation: plain and notched (U-notched) components (see Figure 1 for illustration). Both types of specimens were manufactured using 3D-printer Ultimaker 2 Extended+ with PLA filaments having diameter equal to 2.85 mm. The manufacturing parameters were set as follows: nozzle size 0.4 mm, nozzle temperature 240°C, build-plated temperature 60°C, printing speed 30 mm/s, layer height 0.1 mm, and shell thickness 0.4 mm.

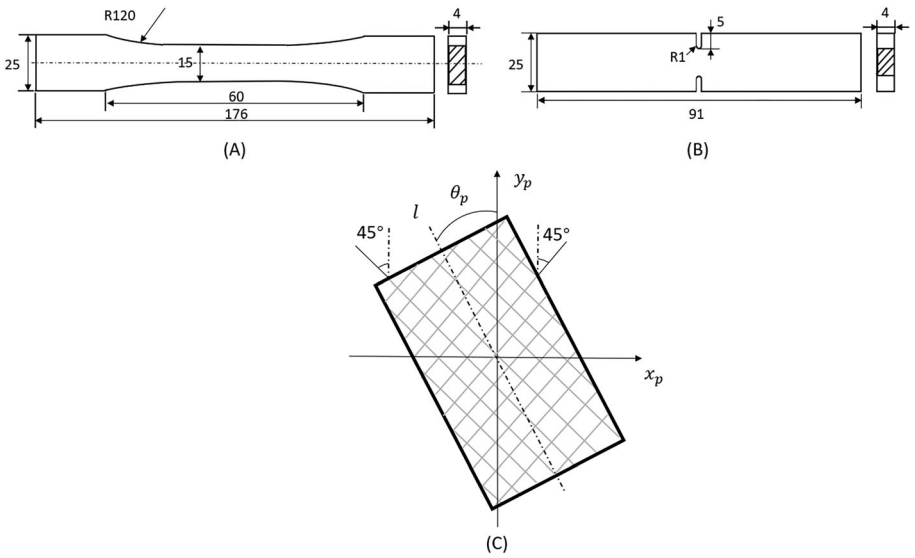

FIGURE 1 3D-printed specimens: (A) the plain specimen geometry; (B) the U-notched specimen with symmetrical U-notch on both longitudinal sides with R1 denoting notch root radius; all values in the figure are in millimeter (mm); (C) manufacturing angle, the diamond-like raster structure and printing direction used for 3D printing

The particular choice of 3D-printed specimens' geometries was dictated by (i) extensive testing of the FIS methodology on relatively simple geometry where the parameters of interest are only manufacturing process parameters (plain specimens in Figure 1A) and (ii) the desire to expand and test the FIS methodology on mixed types of input parameters, that is, manufacturing *and* geometrical/design parameters (U-notched specimens in Figure 1B). The latter potentially will pave the way to a class of design related problems, which is particularly important in industrial applications.

As mentioned earlier, infill density and manufacturing angle were parameters chosen to assess the strength of components. The infill density quantifies the percentage of volume infilled with filaments, and it normally ranges from 10% to 100%. The unfilled space forms manufacturing voids which allow a considerable reduction of material usage and object weight with tolerable sacrifice in general structural strength. It is therefore necessary to assess precisely whether the object being manufactured meets the strength requirements before being used in applications of practical interest.

The manufacturing angle, denoted here as θ_p, is defined as the angle between printing direction y_p (see Figure 1C) and the longitudinal axis l of the specimen. Note that it is different from the raster angle which is the angle between the path of the nozzle and the longitudinal axis of the specimen. This is because the 3D printer used for manufacturing always has a 45° angle between the nozzle path and the longitudinal axis.[19] The nozzle path is marked as crossing lines in Figure 1C, which forms a diamond-like internal structure of the specimen. As such, in the following investigations, the manufacturing angle ranged from 0° to 45° to study of its effect.

All printed specimens were tested using a Shimadzu universal axial machine with a displacement rate of 2 mm/min. Both plain and U-notched specimens were tested up to complete breakage.[19] The results from these experiments will feed into and be presented in later sections.

3 | FUZZY INFERENCE SYSTEM

The main focus of this paper is an introduction and an analysis of an alternative data-driven approach, allowing the estimation of the strength performance of 3D-printed objects. In this section the main aspect of FIS methodology will be discussed in detail for a simplified illustrative example, with attention given to all necessary stages of building up FIS models.

An FIS is based on the theory of fuzzy sets which was first proposed by Zadeh.[20] It can be used to model complicated systems with simple logic rules, similar to human reasoning. The term *fuzzy* refers to indeterministic relationships between the input and the output of an FIS. In this study, the *input* relates to manufacturing and geometrical parameters and the *output* refers to as object's strength performance. The main steps of FIS consist of (i) formulating aforementioned indeterministic relationships, in a form of fuzzy rules, between *known* input and output parameters (historical data) where the process can be considered as the *training* of an FIS and (ii) using this trained FIS to provide an estimation of an *unknown* output (strength performance) for the case of new input (manufacturing and geometrical parameters).

Although there are alternative data-driven methodologies that can be used for estimation such as artificial neural networks,[21] the FIS is popular due to its structural

simplicity. As shown in Figure 2, an FIS is composed of four sections which are *fuzzification*, *fuzzy rule base*, *fuzzy inference engine*, and *defuzzification*. With the assist of fuzzy rules, mapping can be performed between input and output variables, which is in line with human thoughts. The detailed setup of all four FIS components is illustrated below (Sections 3.1–3.4) using, as an example, parameters of 3D printing.

3.1 | Fuzzification

In fuzzification, each input data are mapped according to its degree of membership, ranging from zero to one, and all these membership values together are defined as fuzzy sets. The membership value represents how much the data belongs partially to each subset of a universal set.[22] Numerically, this mapping of each membership value is characterized by membership functions (MF), whose parameters are defined by users.

There are several existing MFs,[23] with the triangular[24] MF being particularly known for its simplicity. It can be expressed mathematically as Equation (1 where users can define the MF by changing parameters, or graphically as Figure 3. In Figure 3, line segments aAc represent the MF of x from a to c where the lower limit (a) and the upper limit (c) both locate the "feet" of the triangle. The MF will reach the peak and be equal to one when x is equal to b ($a < b < c$).

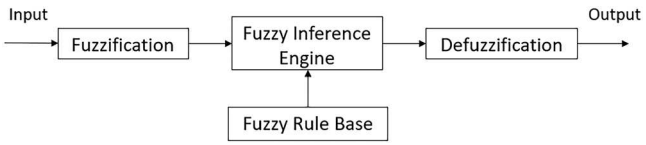

FIGURE 2 Illustration of a fuzzy inference system

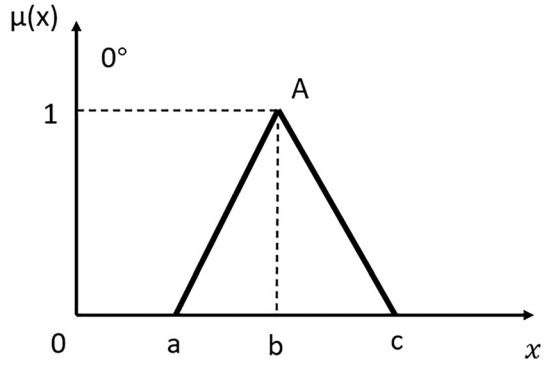

FIGURE 3 Illustration of triangular membership function where x is the input of MF and μ is membership value

$$\mu(x) = \begin{cases} 0, & x \le a \\ \dfrac{x-a}{b-a}, & a < x \le b \\ \dfrac{c-x}{c-b}, & b < x < c \\ 0, & x \ge c \end{cases} \quad (1)$$

To illustrate fuzzification, two 3D-printed parts with 10% and 90% infill densities separately are considered. Here, the infill density is treated as an input variable which will be fuzzified. Assuming the lowest and the highest possible infill densities (known from performed experiments) are 0% and 100%, both 10% and 90% are *high* infill density to some degree. The term *high* here refers to the maximum known infill density 100%. In this case, 90% infill density is significantly *higher* than 10%, that is, it *belongs* to the category *high* significantly more, than 10% infill density *belongs* to the same category. Mathematically, the above phrase can be interpreted using membership values. Following the second row of Equation (1, membership values of 10% and 90% infill density can be calculated. The results of this simple calculation are presented in Figure 4A, showing μ (MF value) for 10% is 0.1 and μ for 90% is 0.9. Note that, for the simplicity of illustration, a is set to be zero and b is equal to 100% infill density in this example. Note also that, in general, triangular MF has a triangular shape, but here, only the left half of the triangle is considered (Figure 4A). This is due to the *high* membership value being defined as 1 when the infill density reaches 100% (i.e., the maximum infill density has the highest potential membership degree). Therefore, there is no need to show the other half of the function which lies out of the range of interest (0–100% infill density).

Similarly, MFs can be formulated to describe how *low* the infill density is. The term *low* refers to the minimum known infill density, in our example 0%. Considering again 10% and 90% infill densities in our 3D-printed parts, we can conclude that the former is considerably *lower* (and its new degree of membership, following the third row of Equation (1, is $\mu = 0.9$) than the latter (with the new degree of membership $\mu = 0.1$), see Figure 4B. Note that here only the right half of the triangle is considered because the highest potential membership value 1 can be achieved at the minimum (*lowest*) infill density 0% and the membership value for 100% infill density is 0.

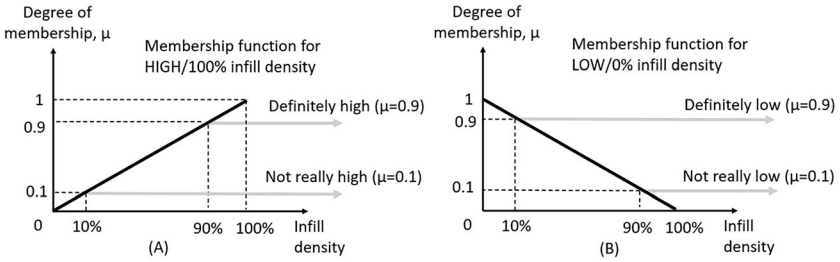

FIGURE 4 Degree of membership versus infill density with triangular membership function for (A) high infill density and (B) low infill density

TABLE 1 Fuzzy rules, illustrative examples

Experiment no.	Infill density (%)	Manufacturing angle (°)	Failure strength (MPa)
1 (fuzzy rule 1)	90	40	10
2 (fuzzy rule 2)	10	0	1
3 (new experiment)	50	30	To be estimated

3.2 | Fuzzy rule base

Fuzzy rule base contains all IF-THEN statements that build connections between inputs and outputs. With existing information or data, the mapping between input and output can be described as inference by these rules. A single rule consists of one or more antecedents and consequents. For example, a fuzzy rule can be a sentence like "if the infill density is *high* (antecedent A) and manufacturing angle is *large* (antecedent B), the failure strength is *large* (consequent)". If the corresponding experimental data, including both manufacturing parameters and failure strength, is already known, the fuzzy rule can also use values directly, for example: "if the infill density is 10% (antecedent A) and the manufacturing angle is 0° (antecedent B), the failure strength of a 3D-printed part is 1 MPa (consequent)." This a typical fuzzy rule that contains two antecedents and one consequent. If another 3D-printed part is known to have infill density of 90%, the manufacturing angle of 40° and failure strength of 10 MPa, a second fuzzy rule can be written as "if the infill density is 90% and the manufacturing angle is 40°, the failure strength is 10 MPa." The detailed parameters and values depend on existing data, and there are normally two or more rules in a fuzzy rule base.

3.3 | Fuzzy inference engine

The input of a fuzzy inference engine is multiple membership values acquired from fuzzification, and the output is one fuzzy set which contains membership values for each output variable. The main body of a fuzzy inference engine contains multiple operations such as *fuzzy operator*, *implication*, and *aggregation*.

To illustrate the working principle of fuzzy inference engine, similar example (as discussed in Section 3.2) will be used. Let us assume that for the two 3D-printed parts, infilled densities, manufacturing angles, and failure strengths are known and formulated as rules 1 and 2 (see Table 1, top two rows); then for the new third 3D-printed part, with the new infill density and the manufacturing angle 50% and 30° respectively, the failure strength are to be estimated using FIS (see Table 1, third row).

3.3.1 | Fuzzy operator*

Following the fuzzification of input values, the degree of membership for each antecedent can be obtained. Generally, a single rule can have multiple input parameters (see Table 1 where both the infill density and the manufacturing angle are present for each rule). In this step, a *fuzzy operator* is applied, that brings together information from aforementioned multiple input parameters to a single value corresponding to a resulting consequent. The standard logical operator *AND* is used at this stage, resulting in a consequent being *true* only when all antecedents are true (i.e., when all input requirements are met).

Mathematically, logical operator *AND* refers here to *minimum (min)* operator, so the output of this operation is the smaller membership value. With input of the FIS in this example being 50% infill density and 30° manufacturing angle, corresponding membership values can be calculated using the second row of Equation (1 as follows:

$$\mu(50\%) = \frac{50-10}{90-10} = 0.5,\ \mu(30^\circ) = \frac{30-0}{40-0} = 0.75 \qquad (2)$$

where the smaller (*min*) membership value is 0.5 (see Figure 5, steps 1 and 2, top row). Note that the infill density in Figure 5 ranges from 10% to 90% not 0% to 100% and that is due to the minimum and the maximum values for a MF here being taken directly from the known experimental data (see fuzzy rules in Table 1). The same comment holds for the manufacturing angle.

3.3.2 | Implication

The outcome of a *fuzzy operator* is a single membership value, and the next step is applying the *implication* method to each fuzzy rule and reshaping the output MF using the obtained single membership value. One of the commonly used implication methods is a truncation, which is again based on AND (*min*) operator (see Figure 5, step 3 at first row).

As introduced at the beginning of Section 3.3, the failure strength ranges from 1 to 10 MPa, and the MF of failure strength is chosen to be triangular, similar to MFs of the infill density and the manufacturing angle.† The term *large* for describing failure strength represents the maximum value which is 10 MPa. Since 0.5 is the *min* membership value in fuzzy operator, the MF of failure strength is truncated by this single value (0.5) and with simple step of bringing 0.5 back into Equation (1, it can be calculated that the failure strength, where the truncation starts, is equal to 5.5 MPa. Note that the input of implication is the single membership value and the output of implication is a fuzzy set (see Figure 5, shadow area from step 3 at first row) relevant to consequent. It can be represented mathematically as $\{\mu_1/x_2,\ \mu_2/x_2,\ ...,\ \mu_n/x_n\}$, here a set of pairs μ_i/x_i represents membership values μ_i of output parameters x_i (values of failure strength). For our example, the fuzzy set can be represented as {0/1, 0.5/5.5, 0.5/10}.

3.3.3 | Aggregation

The final output of FIS is based on considering *all* rules together. In Figure 5, the first row represents fuzzy rule 1, and the second row represents the fuzzy rule 2. Outcomes of each individual rule are *aggregated* so that the result of aggregation is a single fuzzy set. One of the most common aggregation operations is *maximum (max)*, which picks the maximum segments among all MFs and combines them together (see Figure 5, step 4).

In our example, for rule 1, see Equation (2, $\mu(50\%) = 0.5$ and $\mu(30^\circ) = 0.75$, resulting in $\mu_1(50\%\&30^\circ) = \min_1(0.5, 0.75) = 0.5$. For the second rule where the MF describes the low infill density and small manufacturing angle, as explained at the end of Section 3.1, the membership values for both infill density and manufacturing angle are calculated using the third row of Equation (1 as follows:

$$\mu(50\%) = \frac{90-50}{90-10} = 0.5,\ \mu(30^\circ) = \frac{40-30}{40-0} = 0.25 \qquad (3)$$

resulting in $\mu_2(50\%\&30^\circ) = min(0.5, 0.25) = 0.25$.

Since manufacturing angle has the smaller membership value in rule 2, the MF of failure strength for the second row is truncated at 0.25 where failure strength is calculated as 7.75 MPa. Then the *implication* result of the second row in Figure 5 can be represented as {0.25/1, 0.25/7.75, 0/10}.

Thus, inputs of the *aggregation* process are two fuzzy sets acquired from individual *implications* (top two graphs in the fourth column, Figure 5) and the output is a single *aggregated* fuzzy set (bottom graph in the fourth column, Figure 5). The output fuzzy set after aggregation can be represented mathematically as {0.25/1, 0.25/3.25, 0.5/5.5, 0.5/10}.

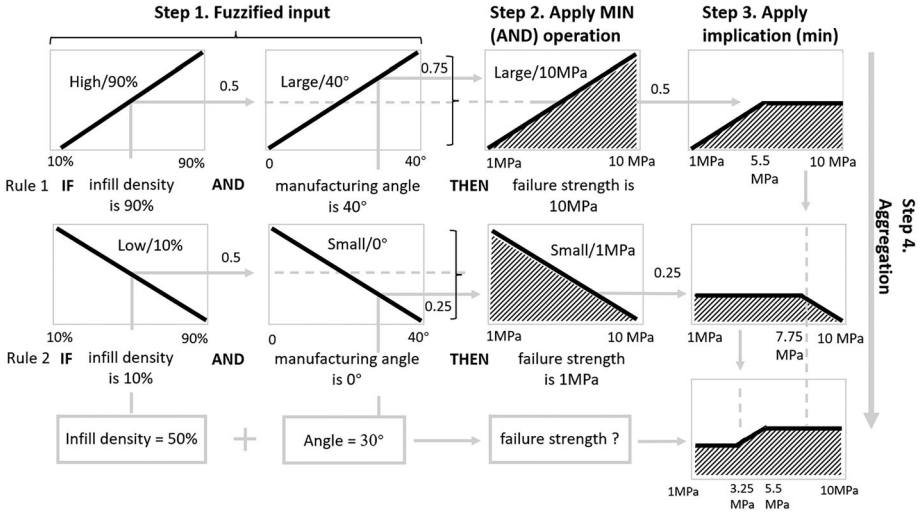

FIGURE 5 Decomposition of a fuzzy inference system

3.4 | Defuzzification

Since the output of fuzzy inference engine is still a fuzzy set (or a number of fuzzy sets if there are more than one output parameters), it is not a "meaningful" value. Defuzzification is the inverse operation of fuzzification, similar to encoding and decoding and the fuzzy sets can be turned into a meaningful value after being defuzzified. There are different types of defuzzification techniques such as center of gravity, mean of maxima, and bisector of area.[25] In this study, the COG technique is chosen since it is most commonly used in practical applications.

The defuzzified value x^* can then be expressed as follows, if the fuzzy set is discrete[26]:

$$x^* = \frac{\sum_{i=1}^{n} \mu(x_i) x_i}{\sum_{i=1}^{n} \mu(x_i)} \tag{4}$$

where $\mu(x_i)$ refers to the membership value of the element x_i (failure strengths) and n is the total number of elements in the sample. Similarly, for continuous MF, the summations in Equation (4 are replaced by integrals. In our example, following simple calculations, $x^* = \frac{\sum_{i=1}^{n} \mu(x_i) x_i}{\sum_{i=1}^{n} \mu(x_i)} \approx 6.1$. In conclusion, the result of defuzzification step is 6.1 MPa which is the estimated failure strength for the 3D-printed part with the infill density 50% and the manufacturing angle 30°.

4 | FIS FOR 3D-PRINTED PLAIN SPECIMENS

In the present and in the following sections, the discussion will return to the analysis of the experimental data obtained from manufacturing and testing the 3D-printed specimens being considered in this study (see Section 2 for details). The construction and the performance of the FIS, following the methodology introduced in Section 3, will now be evaluated using the data from the aforementioned experiments.

4.1 | Manufacturing void size as an additional parameter

As mentioned in Sections 1 and 2, infill density and manufacturing angle are parameters commonly chosen to assess the strength of 3D-printed components. Another parameter, frequently associated with assessing the strength is the size of manufacturing voids.[19] Note, however, that the manufacturing angle θ_p and infill density are independent variables that can be changed individually; contrary to that, the size of manufacturing voids (see Figure 6) depends on the infill density as void sizes will decrease if more internal space are infilled (higher infill density). Therefore, in order to demonstrate the performance of the FIS with multiple interconnected input parameters,[27] the effective size of manufacturing voids, d_v, was included in the research. It was measured by using an optical microscope.[19] In particular, parameter d_v was the calculated average value of measured void sizes which had the same infill density. The analysis based on both infill density and d_v will show whether an additional interconnected parameter can influence the performance of the FIS and which of the two parameters can lead to better accuracy.

4.2 | Experimental results for plain 3D-printed components

The experimental failure strength of plain specimens was calculated as the applied force upon breakage divided by the cross-sectional area of specimens. The calculation was based on the assumption that mechanical strength of a 3D-printed part with infill density lower than 100% can be estimated via an equivalent material which is continuum, homogeneous, linear-elastic, and isotropic.[19] The experimental data are summarized in Table 2 (adapted from Table 1 in Ahmed and Susmel[19]), where θ_p (°) = manufacturing angle, infill density (%), d_v (mm) = size of manufacturing voids, and σ_f (MPa) failure strength. According to experimental investigation discussed in Ahmed and Susmel,[19] 27 combinations of input parameters were tested, with each combination being based on

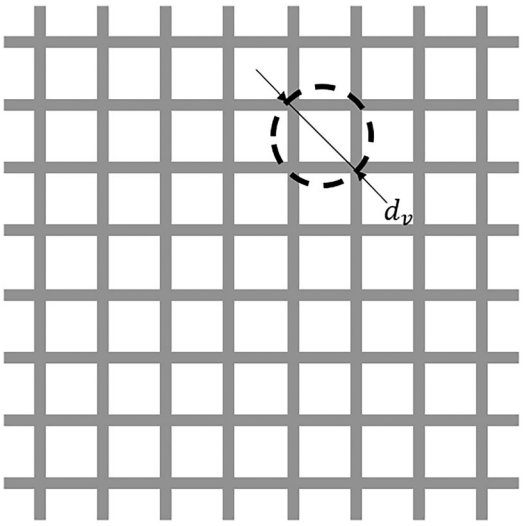

FIGURE 6 Manufacturing voids of a 3D-printed object: Gray lines are printed filaments and blank areas are manufacturing voids

TABLE 2 Summary of experimental results for plain specimens

	Input		Output	
Specimen	θ_p (°)	**Infill density (%)**	d_v **(mm)**	σ_f **(MPa)**
1	0	10	10.7	8.6
2	0	20	4.98	9.2
3	0	30	1.36	10.4
4	0	40	0.88	11.9
5	0	50	0.62	13.6
6	0	60	0.45	16.4
7	0	70	0.33	19.8
8	0	80	0.24	22.5
9	0	90	0.14	25.8
10	30	10	10.72	8.7
11	30	20	5.06	7.9
12	30	30	1.39	9.8
13	30	40	0.96	10.1
14	30	50	0.66	14
15	30	60	0.41	15.9
16	30	70	0.29	18.5
17	30	80	0.25	19.4
18	30	90	0.11	23.4
19	45	10	10.65	8.3
20	45	20	5.12	9.6
21	45	30	1.37	10.8
22	45	40	0.93	12.4
23	45	50	0.65	14.1
24	45	60	0.43	15.8
25	45	70	0.31	18
26	45	80	0.22	20.5
27	45	90	0.13	22.8

three individual tests. For the sake of simplicity, in this paper, an average value of the failure strength for these three tests is calculated and taken as the failure strength of the corresponding input parameter combination. Accordingly, 27 experimental results are presented in Table 2, each of them having a unique combination of manufacturing angle, infill density, the size of manufacturing voids, and the failure strength.

4.3 | Specimens for fuzzy rule base and validation

For examining the performance of the FIS in estimating failure strength properties, a number of results in Table 2 were used for building the necessary fuzzy rules, and the remaining samples were used to validate the estimation accuracy of the FIS. Note that, to minimize the experimental errors, more than one sample was used for validation purposes.

In order to determine the specimens to be used for fuzzy rule base and validation, respectively, 27 specimens were divided into three sections (see dotted lines in Table 2): specimen 1–9, 10–18, and 19–27, respectively (9 specimens in each group). The groups were chosen so that, in each group, manufacturing angles were identical and the infill density ranged from 10 to 90 in sequence. Every *second*, *fourth*, *sixth*, and *eighth* specimens were chosen for validation in each group. For the representativeness of estimation results, the selected validation specimens were evenly distributed in each group. Note that this is not a unique way of choosing validation and

FIS-building specimens, and it has been considered here for convenience reasons. All validation specimens are marked as gray rows in Table 2, and the rest of the specimens are used for building fuzzy rules of the FIS (see Figure 7). Thus, in our case, n is the total number of specimens n is equal to 27, x is the number of specimens used for validation is 12, and the number of specimens used for building fuzzy rules is $n-x=15$.

4.4 | FIS construction

As mentioned in Section 3, one of the main stages in FIS construction is building a fuzzy rule base using existing data. As discussed above, there were 27 data sets in total, where 15 of them were used for building the fuzzy rule base, while the remaining 12 results were used to evaluate the accuracy of estimation (as discussed in Section 4.3 above). In fuzzy rule base, as discussed in Section 3.2, each rule can be presented in the form of "IF-THEN" statements.

To illustrate an example of MFs, Figure 8 presents triangle MFs of one of the manufacturing parameters—manufacturing angle, θ_p. Rather than be in the adjective form of "large, medium, & small", MFs were named with their corresponding parameter values for simplicity of establishing rules.

To clarify MFs presented in Figure 8A, Figure 8B, C, and D shows detailed MFs for all manufacturing angles separately: The MF of manufacturing angle consists of three parts which are 0° (small), 30° (medium), and 45° (large). For example, in Figure 8B, manufacturing angle of 0° has the largest membership value of describing "small manufacturing angle" hence $\mu(x)=1$. However, with increasing the manufacturing angle, it can hardly be represented by the "small angle" category, thus the membership value drops to zero at 30°. Finally, three MFs constitute the general MF of the parameter (Figure 8A).

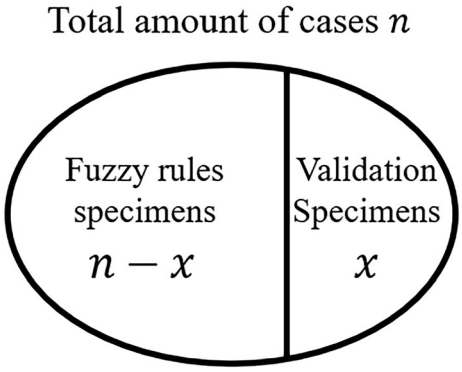

FIGURE 7 Classification of validation and fuzzy rules specimens

4.5 | Estimation results of using FIS

After the FIS being built, the input parameters of validation specimens were fed to the FIS, and the corresponding output was the estimated failure strength. The estimated results were then used to evaluate the accuracy of the FIS, represented by the error calculated as:

$$Error=\left|\frac{\sigma_e-\sigma_f}{\sigma_f}\right|\times 100\% \tag{5}$$

where σ_f is the failure strength recorded in the experiment and σ_e is the value estimated using the FIS. Errors for all validation specimens were then averaged, and this mean value was considered as the estimation error of the FIS.

The detailed experimental and estimation results, together with corresponding errors, are listed in Table 3. Errors for all validation specimens were then averaged, and this mean value was considered as the estimation error of the FIS (7.6%). As can be seen from Table 3, for the case of plain 3D-printed specimens, the FIS produced an accurate (with average error of 7.6%) estimation result.

4.6 | Analysis of results from FIS

Following estimation results of 3D printed plain specimens, presented above, Section 4.6 includes discussions of the effect of specimen numbers and the key manufacturing parameter on estimation accuracy.

4.6.1 | The effect of the number of specimens on estimation accuracy

In order to analyze the effect of experiment quantity " n " on estimation accuracy, three groups of specimens were adapted from Table 2 where the composition of each group were also introduced. Group A had only $n=9$ specimens, group B had $n=18$, and group C had all $n=27$ specimens. The FIS was then applied to Groups A, B, and C separately for estimating failure strength. The contrast of the outcome for all three groups explained the effect of the number of specimens on estimation accuracy. The estimation error for groups A, B, and C were found to be:

A. 9 specimens (specimens 1–9): estimation error 10.3%;
B. 18 specimens (specimens 1–18): estimation error 8.6%;
C. 27 specimens (specimens 1–27): estimation error 7.6* %.

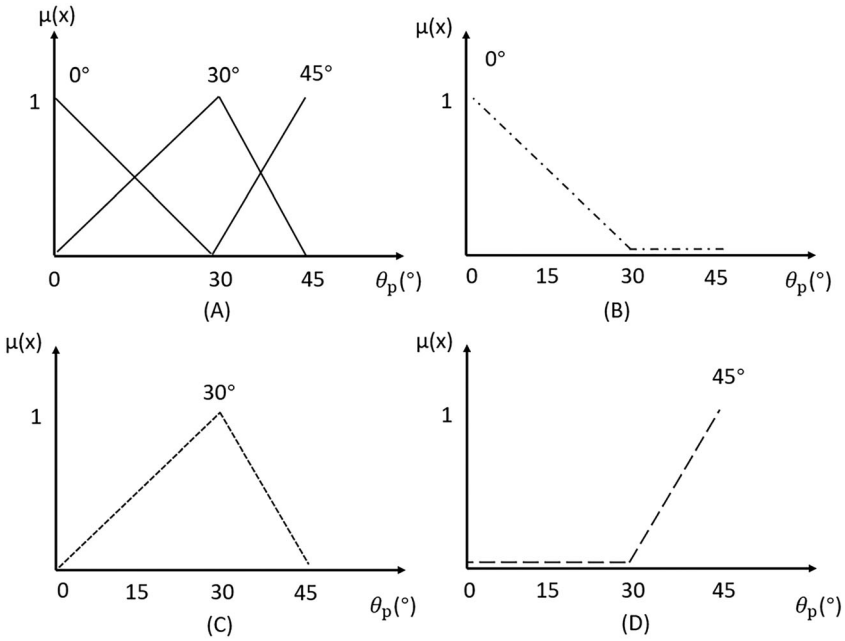

FIGURE 8 (A) Triangular membership functions for manufacturing angle θ_p; (B, C, & D) Decomposition of membership functions for manufacturing angle

TABLE 3 Experimental and estimated results with the error between both results

	Input			Output	Estimation	
Specimen	θ_p (°)	**Infill density (%)**	d_v **(mm)**	σ_f **(MPa)**	σ_e **(MPa)**	**Error (%)**
2	0	20	4.98	9.2	9.9	7.2
4	0	40	0.88	11.9	12.2	2.5
6	0	60	0.45	16.4	17.3	5.5
8	0	80	0.24	22.5	21.8	3.1
11	30	20	5.06	9.3	9.45	1.6
13	30	40	0.96	10.1	10.6	5
15	30	60	0.41	15.9	17.9	12.6
17	30	80	0.25	19.4	21.6	11.3
20	45	20	5.12	9.6	11.4	18.8
22	45	40	0.93	12.4	14	12.9
24	45	60	0.43	15.8	16.3	3.2
26	45	80	0.22	20.5	18.9	7.8
					Average error	**7.6**

As such, it could be concluded that first of all with the given experimental data, the FIS could provide satisfying outcomes for estimating failure strength based on manufacturing angle and infill density with reasonable accuracy. Furthermore, the estimation accuracy improved with the growing number of specimens. However, it has to be said that, from an industrial design point of view, the increment in accuracy from using 9 calibration specimens to using 27 calibration specimens is very little. This suggests that estimates that are accurate from an engineering point of view can be obtained by using a limited number of calibration values. In this context, further study can be focused on the minimum number of experiments required for user-defined estimation accuracy.

4.6.2 | Key manufacturing parameter to the best estimation result

Next, an investigation of the *key* manufacturing parameters was performed. Following Section 4.6.1, for the best

estimation accuracy, group C has been analyzed. The significance of each manufacturing parameter was addressed by evaluating the change of error, while excluding a respectful input variable at a time.[28] It is important to recall here that the estimation error while considering all three parameters (manufacturing angle θ_p, infill density, and manufacturing void size) was found to be 7.6%. Next, without changing θ_p, infill density and d_v were excluded separately in order to study the importance of each of these parameters. The estimation error was found to be equal to 7.1% for considering θ_p & infill density, and 8.2% for considering θ_p & d_v (see Table 4).

It shows the error was smaller than the previously reported, when excluding d_v, that is, the estimation could be more accurate without considering the manufacturing void size as an input parameter of the FIS. On the contrary, the estimation error increased when excluding the infill density, that is, a more accurate estimation result could be achieved when considering the infill density. As mentioned previously, d_v is a function of the infill density as it decreases while the infill density increases. So it is recommended to consider only one of them as the input parameter of the FIS. Analyzing the estimation errors, the infill density can be considered a slightly better choice.

Next, the importance of the manufacturing angle and the infill density were compared. With only θ_p, the FIS gave an estimation error of 40.8%, and with only the infill density, the FIS had an error of 9.3%. As it can be seen, both errors increased considerably, indicating that having only one input parameter could lead to an unaccepted accuracy. Note also that excluding the infill density led to much larger estimation error, thus it can be concluded that for estimating failure strength, it is very important to record the infill density.

Summarizing the above outcomes, the manufacturing void size d_v led to a worse estimation accuracy when using the FIS, whereas both the manufacturing angle, θ_p, and the infill density led to better estimation accuracy and, finally, the infill density had more significance on the estimation result.

5 | FIS FOR 3D-PRINTED U-NOTCHED SPECIMENS

In this section, we will take a further step in evaluating the performance of the FIS by considering two aspects:

i. the ability of the FIS to estimate fracture strength as a function of manufacturing and *geometrical* parameters;
ii. comparison of the FIS performance with analytical methods, used in literature.

In order to address the first question, a new set of experimental data, namely, data for U-notched specimens (Figure 9) were analyzed. Experimental results (adapted from Ahmed and Susmel[19]) are presented in Table 5. A particular choice of the aforementioned data set was dictated by an introduction of a qualitatively new parameter: so far, the discussion circled around the manufacturing input parameters (i.e., the manufacturing angle, the infill density, and the size of manufacturing voids), but the analysis of U-notched specimens would allow to introduce geometrical input characteristics of samples as well.

For the second aim, the FIS performance was compared to the analytical method, based on the equivalent homogenized material concept and the theory of critical distances as proposed in Ahmed and Susmel.[19]

Notched specimens had similar manufacturing and testing processes as discussed in Section 2, but the previously mentioned difference was in sample geometry: new specimens had symmetrical U-shape notches on each longitudinal side (Figure 9). Three different geometries of notched specimens were considered, all had 5-mm notch depth, but the notch radii were 0.5, 1, and 3 mm, respectively.

Similar to previously discussed plain specimens (Section 4), notched specimens also had various combinations of manufacturing angles and infill densities. The varied radius of the notch was added as an extra *geometrical* input parameter. Therefore, for notched specimens, input parameters of the FIS were the manufacturing

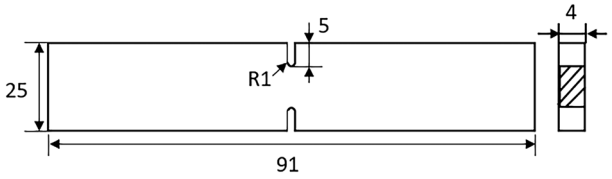

FIGURE 9 The U-notched specimen with symmetrical U-notch on both longitudinal sides where notch root radius R1

TABLE 4 Estimation error (%) versus various input variable combinations

Parameters combination	θ_p, infill density & dv	θ_p & infill density	θ_p & d_v	θ_p	Infill density
Estimation error (%)	7.6	7.1	8.2	40.8	9.3

TABLE 5 Summary of experimental results for U-notched specimens

Specimen	Input			Output
	θ_p (°)	Infill density (%)	Radius (mm)	σ_f (MPa)
1	0	30	0.5	9.7
2	0	30	1	9.5
3	0	30	3	10.9
4	0	50	0.5	13.1
5	0	50	1	13.8
6	0	50	3	14.4
7	0	70	0.5	17.4
8	0	70	1	16.9
9	0	70	3	18.6
10	30	30	0.5	8.2
11	30	30	1	8.5
12	30	30	3	10.0
13	30	50	0.5	11.5
14	30	50	1	12.0
15	30	50	3	12.5
16	30	70	0.5	12.2
17	30	70	1	11.9
18	30	70	3	13.9
19	45	30	0.5	8.0
20	45	30	1	8.1
21	45	30	3	9.8
22	45	50	0.5	11.0
23	45	50	1	11.9
24	45	50	3	13.5
25	45	70	0.5	15.1
26	45	70	1	15.2
27	45	70	3	16.4

angle, the infill density, and the radius of the notch, while the output remained to be failure strength (see Table 5).

Experimental results of U-notched specimens (presented in Table 5) were adapted from Table 2 in Ahmed and Susmel,[19] which contained failure strength of tested parts for different infill density levels, manufacturing angles and radius of notches. Note the difference in infill density: For U-notched analysis, it ranged between 30% and 70% (10% to 90% for the case of plain specimens, discussed in Section 4). As for the output, similar to plain specimens, failure strength was calculated as applied force upon breakage divided by the cross-section area of the breakage.

The total number of 27 manufactured U-notched specimens were considered. The selection of fuzzy rules and validation specimens were chosen to be similar to the one discussed in Section 4.3. Validation specimens were chosen to be specimens 2, 4, 6, 8, 11, 13, 15, 17, 20, 22, 24, and 26, that is, 12 validation specimens (marked as gray rows in Table 5). The remaining 15 specimens (1, 3, 5, 7, 9, 10, 11, 12, 14, 16, 18, 19, 21, 23, 25, and 27) were taken as fuzzy rules.

The comparison between the analytical method and the FIS methodology was based on the accuracy of using both techniques to estimate the failure strength of U-notched specimens. FIS-based estimation errors of failure strength for all 12 validation specimens are presented in Table 6. For the accuracy of the adapted analytical method, error values were directly acquired from Ahmed and Susmel,[19] and these error values are also presented for readers' benefits in

TABLE 6 Error contrast between fuzzy inference system and the adapted analytical method

Specimen	FIS error (%)	Analytical method error (%)
2	0.1	12.5
4	0.2	11.5
6	8.6	15.5
8	2.9	2.1
11	8.7	0.9
13	9.0	5.3
15	7.6	3.6
17	11.7	24.9
20	10.3	5.7
22	5.4	16.4
24	8.6	9.0
26	0.2	5.1
Average	**6.1**	**9.4**

Table 6. It is necessary to point out that the analytical method used the same 12 validation specimens mentioned above.

As it can be seen from Table 6, estimation errors lied within an interval of 11.7% for FIS and 24.9% for the analytical method, respectfully. Note that the maximum estimation error almost was almost halved while using the FIS methodology. Interesting to point out that the average estimation error also decreased from 9.4% (for the analytical method) to 6.1% (for FIS). As such, it can be concluded that the FIS was at least as functional as analytical methods in estimating failure strength and, in the above cases, showed improved accuracy.

As it has been mentioned above, a particular choice to analyze U-notched specimens has been made not only to validate the FIS using existing experimental data and to compare its performance to the existing methodologies but also to test its ability to perform on mixed type of data: manufacturing *and* geometrical input parameters. As it can be seen, the FIS methodology reacted very well (with high accuracy) on the introduction of this new geometrical data. Notch root radius is an important geometrical characteristic, and the FIS approach was shown to be capable of estimating failure strength depending on the radius value (estimations show a similar trend in failure strength as a function of radius, as seen in experiments[19]). Considering the importance of this geometrical characteristic as a possible *design* parameter, it can be concluded that the FIS has a potential to become a simple, robust, and accurate methodology that can be expanded as a *decision-making* tool in design problems.

6 | CONCLUSIONS

In this study, the key steps to be taken to use the FIS were presented and discussed. The FIS-based methodology being formulated was then used to estimate the failure strength of PLA 3D-printed parts. By making use of a large number of experimental data, the performed validation exercise allowed us to demonstrate that the use of this methodology led to reliable and accurate results. It was concluded that more experimental data improve markedly the estimation accuracy. Further studies can be conducted to find out the minimum number of experimental data that are required to reach the wanted estimation accuracy while the costs associated with the calibration process are minimized.

It is important to highlight that, thanks to its intrinsic versatility, the FIS methodology is expected to be equally successful in predicting other mechanical properties such as, for instance, strength under fatigue as well as under dynamic loading. Given the FIS methodology's *modus operandi*, the accuracy in estimating other mechanical responses is obviously expected to increase as the size of the data population used to train the method itself increases.

Compared to other existing approaches, the FIS methodology was seen to offer better performance and higher accuracy. The FIS methodology was tested on different types of input parameters (i.e., manufacturing and geometrical variables) and was seen to be a simple, robust tool that can produce highly accurate estimations. Accordingly, the FIS approach has a great potential as a decision-making tool in design problems. In particular, the FIS approach is expected to be very successful when used together with big data for its calibration. Accordingly, in the near future, this approach could be effectively coupled with 5G, real-time data acquisition technologies, big data streams, artificial intelligence, and automated machine learning to model and predict the mechanical behavior/strength of engineering components and structures.

ACKNOWLEDGMENT

The reported study was funded by the EC Horizon 2020 MSCA-RISE-2016 FRAMED Fracture across Scales and Materials, Processes and Disciplines.

DATA AVAILABILITY STATEMENT

The data that support the findings of this study are available in the supporting information of this article

NOMENCLATURE

d_v effective size of manufacturing voids
n total number of specimens
R notch root radius
y_p printing direction of 3D-printer
θ_p manufacturing angle of 3D printing
μ membership value of corresponding data
σ_f tensile failure strength
σ_e estimated failure strength

ORCID

Ruixuan Tu https://orcid.org/0000-0001-7610-4138
Luca Susmel https://orcid.org/0000-0001-7753-9176

ENDNOTES

* This step and the step below (*implication*) need to be performed for each fuzzy rule (rows in Table 1); however, for clarity of presentation, an example rule (rule 1) will be presented here.

† Note that, although MFs in our example are all triangular for the simplicity of demonstration, both input and output parameters can have different types of MFs in general cases and are determined by users.

REFERENCES

1. Chen Z, Li Z, Li J, et al. 3D printing of ceramics: a review. *J Eur Ceram Soc*. 2019;39(4):661-687.
2. Ribeiro F. 3D printing with metals. *Comput Control Eng J*. 1998;9(1):31-38.
3. Wickramasinghe S, Do T, Tran P. FDM-based 3D printing of polymer and associated composite: a review on mechanical properties, defects and treatments. *Polymers (Basel)*. 2020;12(7):1-42.
4. Gunaydin K, Türkmen SH. Common FDM 3D printing defects. In: *International Congress 3D Printing (Additive Manufacturing Technol Digital India)*; 2018:1-8.
5. Masood SH. Advances in fused deposition modeling. *Compr Mater Process*. 2014;10:69-91.
6. Dwiyati ST, Kholil A, Riyadi R, Putra SE. Influence of layer thickness and 3D printing direction on tensile properties of ABS material. *J Phys Conf Ser*. 2019;1402(6):066014.
7. Chacón JM, Caminero MA, García-Plaza E, Núñez PJ. Additive manufacturing of PLA structures using fused deposition modelling: effect of process parameters on mechanical properties and their optimal selection. *Mater Des*. 2017;124:143-157.
8. Yousefi A. A. Effects of 3D printer nozzle head temperature on the physical and mechanical properties of PLA based product. In *12th International Seminar on Polymer Science and Technology*. 2016:3-5.
9. Nurizada A, Kirane K. Induced anisotropy in the fracturing behavior of 3D printed parts analyzed by the size effect method. *Eng Fract Mech*. 2020;239:107304.
10. Floor J, Van Deursen B, Tempelman E. Tensile strength of 3D printed materials: review and reassessment of test parameters. *Mater Test*. 2018;60(7–8):679-686.
11. Mirsayar MM. A generalized criterion for fatigue crack growth in additively manufactured materials—build orientation and geometry effects. *Int J Fatigue*. 2021;145:106099.
12. Ezeh OH, Susmel L. Fatigue strength of additively manufactured polylactide (PLA): effect of raster angle and non-zero mean stresses. *Int J Fatigue*. 2019;126:319-326.
13. Wang Y, Wang W, Susmel L. Constant/variable amplitude multiaxial notch fatigue of additively manufactured AISI 316L. *Int J Fatigue*. 2021;152:106412.
14. Ezeh OH, Susmel L. Reference strength values to design against static and fatigue loading polylactide additively manufactured with in-fill level equal to 100%. *Mater des Process Commun*. 2019;1:e45.
15. Ng CT, Susmel L. Notch static strength of additively manufactured acrylonitrile butadiene styrene (ABS). *Addit Manuf*. 2020;34:101212.
16. Ziemian C, Sharma M, Ziemian S. Anisotropic mechanical properties of ABS parts fabricated by fused deposition modelling. In: Gokcek M, ed. *Mechanical Engineering*. InTech; 2012:159-180.
17. Koch C, Van Hulle L, Rudolph N. Investigation of mechanical anisotropy of the fused filament fabrication process via customized tool path generation. *Addit Manuf*. 2017;16:138-145.
18. Yerbolat G, Shynggys A, Ali MH. Mechanical property prediction method based on multi-material 3D printer. In: *2018 Joint 7th International Conference on Informatics, Electronics and Vision and 2nd International Conference on Imaging, Vision and Pattern Recognition, ICIEV-IVPR 2018*. Institute of Electrical and Electronics Engineers Inc.; 2019:498-502.
19. Ahmed AA, Susmel L. Static assessment of plain/notched polylactide (PLA) 3D-printed with different infill levels: equivalent homogenised material concept and theory of critical distances. *Fatigue Fract Eng Mater Struct*. 2019;42(4):883-904.
20. Zadeh LA. Fuzzy sets. *Infect Control*. 1965;8(3):338-353.
21. Özcan F, Atiş CD, Karahan O, Uncuoğlu E, Tanyildizi H. Comparison of artificial neural network and fuzzy logic models for prediction of long-term compressive strength of silica fume concrete. *Adv Eng Softw*. 2009;40(9):856-863.
22. Akkurt S, Tayfur G, Can S. Fuzzy logic model for the prediction of cement compressive strength. *Cem Concr Res*. 2004;34(8):1429-1433.
23. Zhao J, Bose BK. Evaluation of membership functions for fuzzy logic controlled induction motor drive. *IECON Proc (Industrial Electron Conf)*. 2002;1:229-234.
24. Princy S, Dhenakaran SS. Comparison of triangular and trapezoidal fuzzy membership function. *J Comput Sci Eng*. 2016;2:46-51.
25. Saletic DZ, Velasevic DM, Mastorakis NE. Analysis of basic defuzzification techniques. *Recent Adv Comput Comput Commun*. 2002;247-252.
26. Gitman IM, Klyuev AV, Gitman MB, Stolbov VY. Multi-scale approach for strength properties estimation in functional materials. *ZAMM Zeitschrift fur Angew Math Und Mech*. 2018;98(6):945-953.
27. Gitman IM, Gitman MB, Batin SE, Boyarshinov DA. Stochastic stability of performance properties for materials with non-

deterministic microstructure. *ZAMM Zeitschrift fur Angew Math Und Mech*. 2020;101(6):1-18.

28. Gitman IM, Gitman MB, Stolbov VY, Batin SE, Boyarshinov DA. Methodology to estimate the minimum number of experiments and key microstructural parameters in macroscopic strength properties evaluation. *ZAMM Zeitschrift fur Angew Math Und Mech*. 2019;99(3):1-9.

How to cite this article: Tu R, Gitman I, Susmel L. Fuzzy inference system for failure strength estimation of plain and notched 3D-printed polylactide components. *Fatigue Fract Eng Mater Struct*. 2022;1-15. doi:10.1111/ffe.13689